4

HI Absorption study towards Galactic Center and Anticenter

A few observation and much reasoning lead to error;
many observations and a little reasoning to truth.

—Alexis Carrel

Summary and the main results of chapter 4

Early HI 21cm-line absorption measurements towards the Galactic Center using the Parkes Interferometer suggested the existence of a low optical depth (τ_{peak} ∼0.3), broad (σ_v ∼35 km s^{-1}) feature centered at zero LSR velocity. This was attributed to a population of weakly absorbing fast interstellar clouds. However, later observations carried out to verify this using the Westerbork Synthesis Radio Telescope gave negative results. In an attempt to resolve this long-standing and important issue, we have made new HI 21cm-line absorption measurements towards the Galactic Center using the Australia Telescope Compact Array and towards the Galactic Anticenter using the Westerbork Synthesis Radio Telescope. This chapter discusses the results obtained from our investigations. The main results are:

- ***We see clear evidence for the presence of a wide HI absorption feature, with a peak optical depth τ_{HI} ∼0.31 and dispersion σ_v ∼50 km s^{-1}.***
- ***We conclude that the Westerbork observations failed to detect this feature due to the insufficient bandwidth used for their observations.***
- ***No such feature was detected towards the Galactic Anticenter down to a 3σ limit of 0.006 in optical depth.***

4.1 INTRODUCTION

About 20 years ago, Radhakrishnan and Sarma (1980) carried out a Gaussian fitting analysis to the HI 21cm-line optical depth profile towards the Galactic Center obtained with the Parkes Interferometer by Radhakrishnan et. al. (1972). The HI absorption towards the Galactic Center is saturated near zero LSR velocities (See Fig. 4.1). The central velocity of this component obtained from a Gaussian fit to its wings coincides with the zero of the velocity with respect to the LSR. **Since this direction is free from the radial velocities arising from the differential Galactic rotation, the peculiar motions of HI clouds in the Galaxy can be measured directly along this line of sight**. Hence one would expect this feature to arise from the superposition of absorption from a large number of clouds located along the line of sight. The width of this feature should therefore represent a measure of the velocity dispersion of the clouds. The derived width $\sim$ 5 km s^{-1} agreed well with that inferred from the HI 21cm-line observations in other directions of the Galaxy (see, for example, Crovisier, 1978). Radhakrishnan and Sarma also found evidence for an unexpectedly wide (σ_v $\sim$ 35 km s^{-1}) low optical depth ($\tau_{HI} \sim 0.3$) feature, also centered at the zero velocity with respect to the LSR. The extraordinary width of this absorption feature led them to the conclusion that it cannot be due to an isolated concentration of gas, rather this may be due to a collection of clouds distributed over the long pathlength towards the Galactic Center.

A detailed interpretation of the distribution of peculiar velocities of the Interstellar clouds was done by Radhakrishnan and Srinivasan (1980). They identified this shallow but wide HI absorption feature with an ensemble of low optical depth clouds distributed in the Galaxy. They speculated about the existence of two kinds of HI clouds: (i) Optically thick clouds with a small velocity dispersion, and (ii) a second population of relatively low column density and faster clouds ($N_{HI} \sim 5$–10×10^{19} cm^{-2}, $\sigma_v \sim$ 35 km s^{-1}) To support this argument, they compared the optical and radio observations of the ISM. The optical observations were extensively referred to in the previous chapter. Radhakrishnan and Srinivasan compared the folded version of the optical depth profile towards SgrA with a histogram constructed from Siluk and Silk's data (Siluk and Silk, 1974). From the similarity of these, they concluded that the same population is responsible for the large spread in velocities in both cases. They suggested that because of their low column density these clouds would have been difficult to detect in HI emission, thus explaining why the earlier attempts had failed to detect HI emission corresponding to the high velocity CaII absorption lines towards bright stars (See for example, Rajagopal et. al., 1998 and the references therein). Radhakrishnan and Srinivasan concluded that the distance to the Galactic Center ($\sim$ 8 kpc) being much larger than the distance to nearby bright stars for which the CaII absorption data is available ($\lesssim$ 2 kpc), it enables the HI absorption from individual clouds to build up to an observable peak towards the Galactic Center. The only other direction which has this advantage is the Galactic Anticenter.

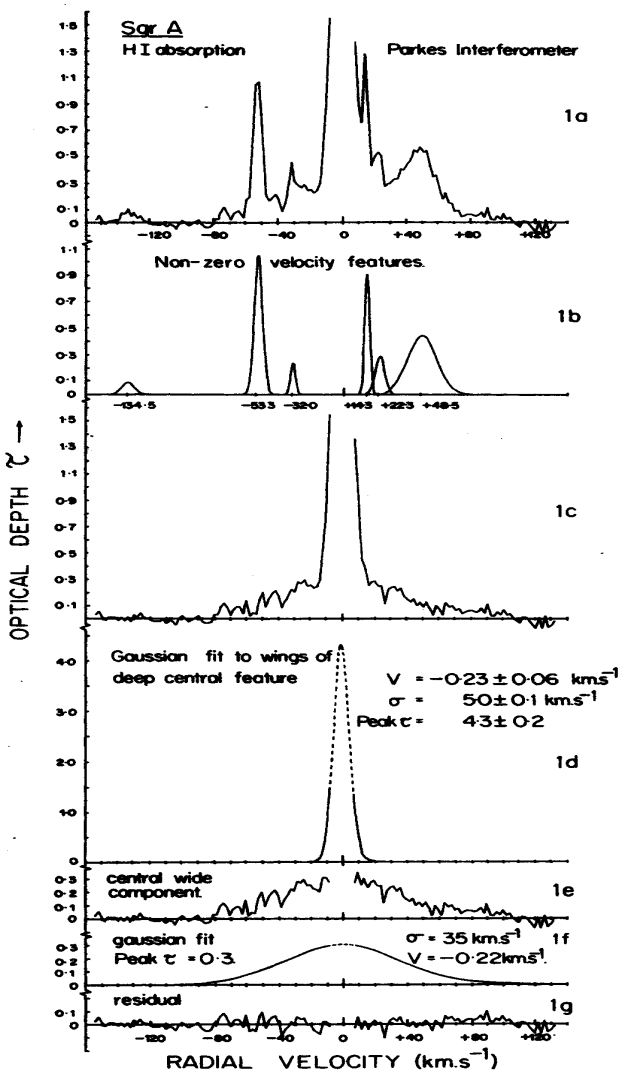

Fig. 4.1 The HI optical depth profi le towards the Galactic center and its progressive decomposition to individual Gaussian features (From Radhakrishnan & Sarma, 1980)

The implications of this scenario, if true, are significant. If the large velocity dispersion clouds are representative of a true Galactic population, then the integrated column density of the clouds would imply a total mass in these clouds twice that of the normal population of clouds. Given the ratio of their velocity dispersions, the kinetic energy of the low optical depth clouds would be ~ 100 times that of the denser clouds (Radhakrishnan and Srinivasan, 1980). However, Schwarz, Ekers and Goss (1982) measured HI absorption towards the Galactic Center using the Westerbork Synthesis Radio Telescope and they concluded that their observations did not reveal the wide HI absorption feature reported by Radhakrishnan and Srinivasan. However, support for a high velocity tail came from an independent study **comparing the terminal velocities of HI absorption spectra in the directions of 38 HII regions with their Radio Recombination Line velocities** (Anantharamaiah et al., 1985). Kulkarni and Fich (1985) found some evidence for large velocity dispersion HI clouds, but they were more cautious than Radhakrishnan and Srinivasan about their filling factor.

4.1.1 Motivations for the present Observations

Thus the possible existence of large peculiar velocity HI clouds in the Galaxy remained contentious. But surprisingly there were no further efforts to resolve it. We have revisited this problem by **imaging the Galactic Center in HI absorption using the Australia Telescope Compact Array (ATCA), and the Galactic Anticenter using the Westerbork Synthesis Radio Telescope (WSRT)**. The main purpose of the present observations was to resolve this issue. In the next section we present an overview of the Galactic center complex. Section 4.3 describes the observational setup. Results are presented in sect. 4.4, followed by a discussion section 4.5

4.2 THE GALACTIC CENTER: AN OVERVIEW

The region bounded by the inner tens of light years at the center of the Milky way Galaxy contains five principal components that co-exist within the central deep well of Gravitational potential. These constituents are the black hole candidate SgrA* with a mass equivalent to $2.6 \pm 0.2 \times 10^6$ M$_\odot$, a surrounding cluster of evolved stars, a complex of young stars, molecular and ionized gas clouds and a powerful supernova remnant. The accretion of stellar winds by SgrA* appears to produce far less radiation than indicated by estimates based on models of Galactic nuclei. The radio continuum flux in this complex exceeds 150 Jy at 20cm wavelength. We briefly explain the radio sources in the SgrA complex below.

4.2.1 The massive black hole candidate SgrA*

SgrA*, the bright compact radio source at the dynamical center of the Galaxy, discovered by Balick & Brown (1974) at 1.4GHz, has a flux density of $\sim$800 mJy. Proper motion studies of stars in the neighbourhood of SgrA* provides a mass of $(2.6 \pm 0.2) \times 10^6$ to lie within the inner 0.015 pc of the Galactic center (Genzel et al, 1996 and references therein). VLBA observations with milliarcsecond resolution show that the angular radius of SgrA* is 0.76 ± 0.04 mas, which at a distance of 8 kpc translates to about 4 AU (Bower & Backer, 1998). The present understanding is that SgrA* is a massive black hole (Genzel et al, 1996). The only viable alternative being a distributed population of $\sim$10 $M_\odot$ black holes. Whether such a concentration is stable against mergers, eventually producing a single massive object is still an open question.

4.2.2 The thermal source SgrA West

The picture that has emerged from the multi wavelength studies of the Galactic center is that there exists a molecular disk - the circum nuclear disk (CND) with a mass $> 10^4$ $M_\odot$. Within the cavity of molecular gas in the CND lies the ionized gas, known as SgrA West, which appears like a three armed spiral like structure orbiting around SgrA*. The kinematics of ionized gas surrounding SgrA* shows systematic velocities along various components of SgrA W ($\sim 30''$ west of SgrA*), with a radial velocity structure that varies regularly between –100 km s^{-1} and +100 km s^{-1} in south-north direction. The velocities within the inner $10''$ becomes increasingly more negative down to $\sim$350 km s^{-1} towards SgrA* (Yusef-Zadeh et al, 1989; Roberts et al, 1996).

4.2.3 The non thermal source SgrA East

Away from the Galactic center, to a scale of 10-20 pc, radio continuum observations show a prominent, non thermal, shell like structure known as SgrA East. This extended source is superposed onto the thermal source SgrA W and the CND. Low frequency radio continuum observations show a decrease in the brightness of SgrA E shell at the position of SgrA W, which results from foreground free-free absorption. Therefore, a good portion of SgrA E must lie behind SgrA W (Yusef-Zadeh & Morris, 1987; Pedlar et al, 1989).

4.2.4 The +50 km s^{-1} Molecular cloud

One component of the molecular gas distribution in the SgrA complex occurs at 40 - 60 km s^{-1}. This is known as the "50 km s^{-1} cloud". SgrA E, although lying almost entirely behind the Galactic center, is close enough to partially envelop SgrA W and the high pressure associated with this remnant is sufficient to disturb the nearby 50 km s^{-1} cloud. The initial evidence for the interaction came from CO observations of

Table 4.1 Observational setup

Direction	Galactic Center	Anticenter
Telescope	ATCA	WSRT
Configuration	1.5D	
Synth. beam	$56^{''} \times 23^{''}$@ –0.7°	$45^{''} \times 20^{''}$@ +4°
Baseband width	4.0 MHz	2.5 MHz
No. of Channels	2048	256
Velocity Res.	0.8 km s^{-1}	4 km s^{-1}
Integration. time	$\sim$ 10 hr	3 hr/source
Observing dates	April 2000	May 1999

the molecular cloud. Further molecular line observations clearly showed a velocity gradient consistent with acceleration by SgrA E (Serabyn et al, 1992). More recent, higher resolution studies of the ammonia molecule have confirmed these ideas and suggest that the gas is warmer as a result of this disturbance (Coil and Ho, 1999).

4.3 OBSERVATIONS AND DATA REDUCTION

4.3.1 Galactic Center

We have imaged the Galactic Center region using the Australia Telescope Compact Array (ATCA). The velocity spread in the HI 21cm-line absorption features towards the Galactic Center is –200 km $s^{-1} \lesssim V_{lsr} \lesssim$ +140 km s^{-1} (Liszt et. al., 1983). *A good spectral baseline and a stable bandpass are crucial to search for a wide and shallow absorption feature. In addition, a high spectral resolution is needed to fit and subtract the narrow HI absorption lines.* ***Hence, we have used a 4 MHz bandwidth ($\sim$ 845 km s^{-1}) and 2048 channels ($\Delta v \sim$ 0.8 km s^{-1} after Hanning smoothing) for our observations***. The ATCA was used in the configuration 1.5D, which has baselines in the range 104 m – 1439 m. We used frequency switching on-source for the bandpass calibration. Phase and amplitude calibration were carried out once an hour. The total observing time was 24 hours, spread over two days and the total integration time with the center frequency on the HI line was $\sim$ 10 hours. A summary of the observational setup is listed in Table 4.1.

The data reduction was carried out using the *Multi Channel Image Reduction Image Analysis and Display* (MIRIAD) package. Continuum subtraction was carried out by fitting a linear baseline to the line-free channels as a function of frequency in the visibility domain and subtracting the best fit continuum from all the channels. Imaging and deconvolution were carried out using the *Astronomical Image Processing*

Software (AIPS). Images with different u-v ranges were made to convince ourselves that there was no contamination due to HI emission. This was satisfactory except for a few channels. **We have also made separate spectral cubes with velocity resolution and synthesized beams matching the Parkes Interferometer setup used by Radhakrishnan and Sarma, 1980 (Bandwidth of 1.5MHz at Δv = 2 km s^{-1}) and the WSRT setup used by Schwarz et al., 1982 (Bandwidth of 1.25 MHz at Δv = 4.1 km s^{-1})**. Finally, the Gaussian fitting was carried out using our own code, as well as with the *Groningen Image Processing System* (GIPSY).

An important point to keep in mind is that HI self absorption is widespread in the Galactic plane. One can expect self absorption to be important towards the Galactic center. However, in our analysis we have not made any attempt to model the possible self absorption.

4.3.2 Galactic Anticenter

We have measured HI absorption using the WSRT towards two extragalactic radio sources: 4C+29.19 (l = 179.88, b = +0.01, $S_{20cm} \sim$ 980 mJy) and 4C+28.16 (l = 179.68, b = –0.93, $S_{20cm} \sim$ 520 mJy) located within half a degree from the Galactic Anticenter. A summary of the observational setup is listed in Table 4.1. As in the case of ATCA observations, bandpass estimation was carried out using frequency switching on source. The total observation time was 14 hours. The data reduction was carried out in AIPS. Gaussian fitting analysis of the HI optical depth profiles were carried out using GIPSY.

4.4 ANALYSIS AND RESULTS

4.4.1 New evidence for the Wide Absorption Feature

The optical depth profile obtained from our ATCA observations towards the peak brightness in SgrA region is shown in Figure 4.2.a. Note that the central feature at $V_{lsr} \sim$ 0 km s^{-1} is saturated. A visual inspection of the spectrum straightaway reveals 14 narrow unsaturated features ($\sigma_v \lesssim$ 10 km s^{-1}). In addition, there is the central saturated absorption feature. We attempted to fit the observed optical depth profile with 15 gaussians, each representing one of the absorption features referred to above. With specific reference to the central saturated feature, we used only the wings of a gaussian with $\tau < 2.0$. The fitting procedure used a non-linear least squares fit algorithm based on the Levenberg-Marquardt method (Press et al., 1992). The initial guesses - the central velocities, the peak optical depths and the standard deviations of each of the 15 gaussians - were iterated simultaneously to obtain the minimum reduced chi-squared value for the fit. All of the channels were given uniform weights. These model gaussians are shown in Figure 4.2.b1 (unsaturated gaussian features)

Table 4.2 Parameters of the 15 individual Gaussian components fitted to the HI optical depth profile towards SgrA.

No.	Central velocity V_{lsr} (km s^{-1})	Peak τ_{HI}	σ_v (km s^{-1})
1	-132.679 $\pm$ 0.2	0.13 $\pm$ 0.04	8.9 $\pm$ 0.9
2	-74.58 $\pm$ 0.09	0.27 $\pm$ 0.06	4.2 $\pm$ 0.1
3	-61.44 $\pm$ 0.07	0.36 $\pm$ 0.05	2.6 $\pm$ 0.1
4	-53.41 $\pm$ 0.02	1.45 $\pm$ 0.02	2.45 $\pm$ 0.03
5	-44.35 $\pm$ 0.07	0.36 $\pm$ 0.04	4.12 $\pm$ 0.04
6	-32.02 $\pm$ 0.05	0.49 $\pm$ 0.04	2.21 $\pm$ 0.07
7	-23.66 $\pm$ 0.05	0.5 $\pm$ 0.4	4.89 $\pm$ 0.07
8	-17.2 $\pm$ 0.1	0.2 $\pm$ 0.02	1.0 $\pm$ 0.2
9	0.597 $\pm$ 0.008	3.4 $\pm$ 0.8	6.1 $\pm$ 0.8
10	15.77 $\pm$ 0.06	0.46 $\pm$ 0.06	1.20 $\pm$ 0.08
11	21.6 $\pm$0.3	0.200 $\pm$ 0.04	2.6 $\pm$ 0.1
12	26.6 $\pm$0.1	0.33 $\pm$ 0.01	5.95 $\pm$ 0.05
13	44.68 $\pm$ 0.07	0.35 $\pm$ 0.07	26 $\pm$ 2
14	50.7 $\pm$0.5	0.05 $\pm$ 0.04	1.4 $\pm$ 0.4
15	102.5 $\pm$0.3	0.08 $\pm$ 0.06	11 $\pm$ 1

and 4.2.b2 (the saturated gaussian near $V_{lsr} \sim 0$ km s^{-1}). For the sake of clarity, the saturated component is shown separately. The best fit values are given in Table 4.2. The minimum value of reduced Chi-squared obtained was 3.8. Figure 4.2.c shows the residual spectrum when the best fit model spectrum with 15 gaussians was subtracted from the observed spectrum. It may be seen that the residual spectrum shows **systematic deviations** at 5σ level. Thus one is left to contend with these residuals.

The fitting procedure was repeated, this time with 16 components, with a guess for an additional component centered near zero LSR velocity. The best fit resulted in a reduced Chi-square value of 2.9, and this is shown in Figure 4.3, and the best fit values of these 16 gaussian components are given in Table 4.3. Like before, the best fit model gaussians are shown in Figure 4.3.b1 and 4.3.b2. The additional wide gaussian component centered near zero LSR velocity is shown separately in 4.3.b3. The residual after subtracting the best fit model spectrum with 16 gaussians from the observed spectrum is shown in Figure 4.3.c. This clearly has no significant **systematic deviations**, unlike the residuals shown in Figure 4.2.c.

It is noticeable from Fig. 4.3.c that the *rms* in the residual is larger near zero LSR velocities. The extended HI emission entering the *primary beam* can result in

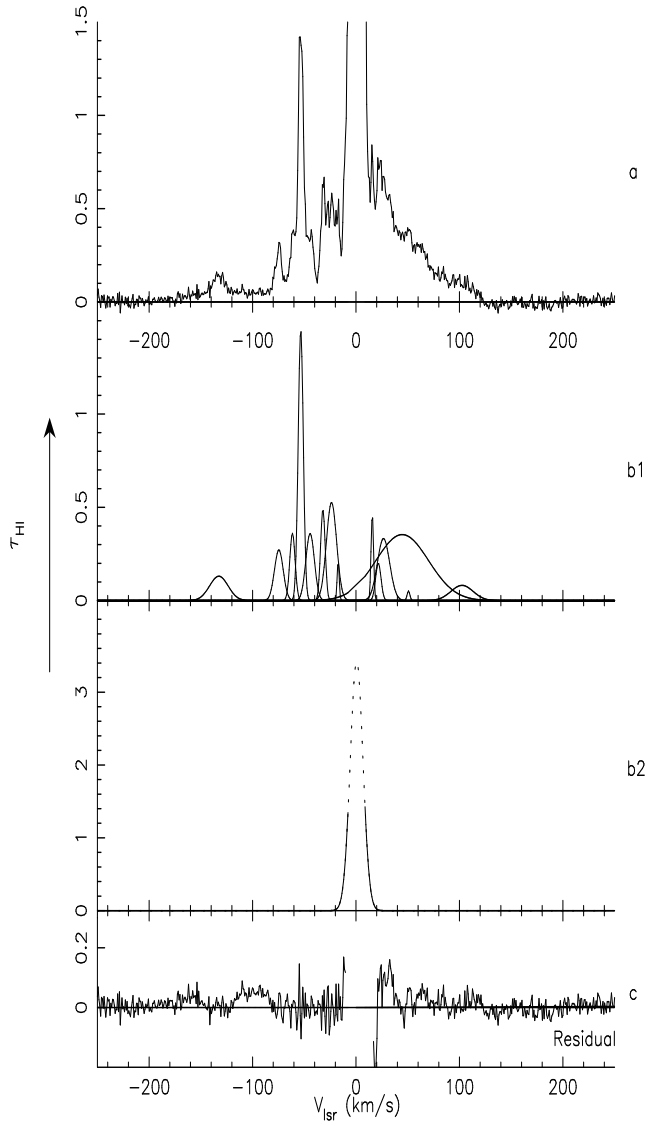

Fig. 4.2 The results of the 15 component gaussian fit to the HI optical depth spectrum. (a) The optical depth profile towards SgrA from the ATCA Observations. (b1) The best fit models for the unsaturated gaussian features. (b2) The gaussian model for the central saturated component and (c) The residual spectrum. Notice the systematic deviations in the residual.

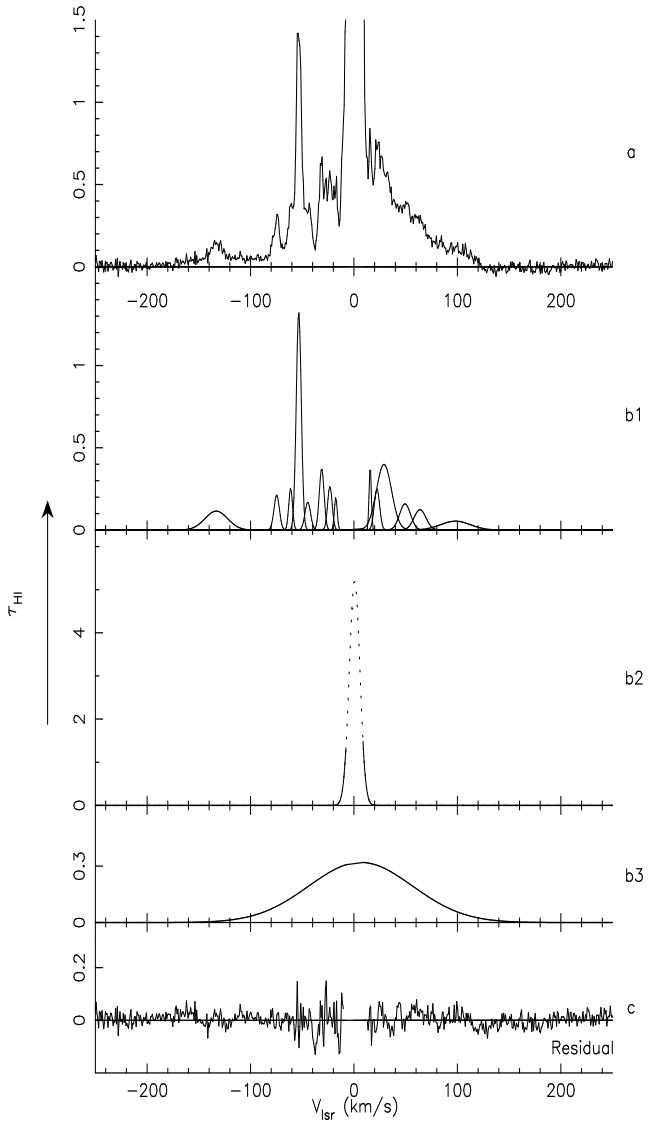

Fig. 4.3 The results of the 16 component gaussian fit to the HI optical depth spectrum. (a) The optical depth profile towards SgrA from the ATCA Observations. (b1) The best fit models for the unsaturated gaussian features. (b2) The gaussian model for the central saturated component. (b3) The gaussian model for the central wide component and (c) The residual spectrum. The systematic deviations in the residual, seen in Figure 4.2.c is absent now.

Table 4.3 Parameters of the 16 individual Gaussian components fitted to the HI optical depth profile towards SgrA. The component no. 10 is the wide Gaussian component.

No.	Central velocity V_{lsr} (km s^{-1})	Peak τ_{HI}	σ_v (km s^{-1})
1	–133.1 ± 0.7	0.12 ± 0.01	10.9 ± 0.5
2	–74.7 ± 0.3	0.21 ± 0.02	2.6 ± 0.3
3	–61.2 ± 0.2	0.25 ± 0.04	1.8 ± 0.2
4	–53.4 ± 0.1	1.33 ± 0.02	2.4 ± 0.1
5	–44.7 ± 0.4	0.17 ± 0.02	2.7 ± 0.4
6	–31.2 ± 0.1	0.37 ± 0.04	2.3 ± 0.2
7	–23.3 ± 0.5	0.27 ± 0.02	2.3 ± 0.6
8	–17.6 ± 0.1	0.20 ± 0.04	1.4 ± 0.1
9	+0.63 ± 0.06	5.2 ± 0.2	5.10 ± 0.03
10	**+7 ± 2**	**0.32 ± 0.02**	**50 ± 3**
11	+15.7 ± 0.1	0.39 ± 0.06	1.1 ± 0.1
12	+22.2 ± 0.4	0.25 ± 0.02	2.6 ± 0.7
13	+29 ± 2.8	0.30 ± 0.02	7.3 ± 0.4
14	+49 ± 1.2	0.16 ± 0.03	5 ± 2
15	+64 ± 1.4	0.12 ± 0.02	6 ± 1
16	+98 ± 1.9	0.05 ± 0.04	14 ± 2

an enhanced system temperature in the corresponding channels and hence larger rms noise in those channels. The emission towards the Galactic Center as detected by a single dish used in the Leiden-Dwingeloo Sky Survey (Hartmann & Burton, 1995) reveals the HI emission reaching a peak brightness temperature $T_B \sim 70$K at $V_{lsr} \sim$ –16 km s^{-1}. T_B is more than $\sim$ 20K in the entire range –25 km s^{-1} $\lesssim V_{lsr} \lesssim$ +25 km s^{-1}. For the ATCA, this contribution from emission would increase the expected rms noise in these channels by a factor of ~ 1.5.

Let us now, for a moment, discuss the significant "negative optical depths" in the residual. The peak T_B of 70K at $V_{lsr} \sim$ –16 km s^{-1} seems to be correlated with the large negative feature at this velocity. The second pronounced negative in the residual at $V_{lsr} \sim$ –37 km s^{-1} coincides with the HI emission at this velocity with T_B reaching $\sim$ 8K. The apparent negative optical depths in these channels, $\sim$ –0.08 and –0.13, respectively, can be due to the HI emission being detected by the *synthesized beam*. Indeed, we do find pixels in our line image away from the background continuum source (SgrA W) where the measured flux densities at these channels are $\sim$ 120 and 150 mJy beam^{-1}. These were also found to be distinctly above the rms noise level in these channels. These values (120 & 150 mJy beam^{-1}) above the continuum flux of the background source ($\sim$ 1.3 Jy beam^{-1}) imply an apparent optical depth $\sim$ –0.09 and –0.12 respectively. The rms in HI optical depth in both these channels are ~ 0.03. **Hence, one can expect the HI emission detected through the synthesized beam to be responsible for the negative values in the optical depth profile discussed here**.

As we mentioned earlier, the Parkes Interferometer observations (Radhakrishnan and Sarma, 1980) had suggested a wide HI absorption component with $\sigma_v \sim 35$ km s^{-1}. The width of the wide line estimated from our analysis is larger and is $\sim$50 km s^{-1} as may be seen from Fig. 4.3 and Table 4.3. Having noted this, we do not at present wish to attach any great significance to this. However, the peak optical depth values agree to within 7%. In addition, the central velocity of this feature was found to be at $V_{lsr} \sim 0$ km s^{-1} by Radhakrishnan and Sarma, but our estimate gives $V_{lsr} \sim$ 7 km s^{-1}. However, the parameters for the central saturated component obtained by us (No.9 in Table 4.3) are in good agreement (within 10%) with the results obtained by Radhakrishnan and Sarma, as well as that obtained by Schwarz et al (1982). In the following sections, we compare our results with these two earlier but conflicting observations.

4.4.2 Comparison with the Parkes Interferometer results

The Parkes Interferometer observations (Radhakrishnan et al., 1972) were carried out with a baseline of 120 m, a bandwidth of 1.5 MHz ($\sim$ 316 km s^{-1}) and a velocity resolution of $\sim$ 2 km s^{-1}. The corresponding numbers in the present observations are: maximum baseline of 1.5 km, bandwidth of 4 MHz and velocity resolution of 0.8 km s^{-1}

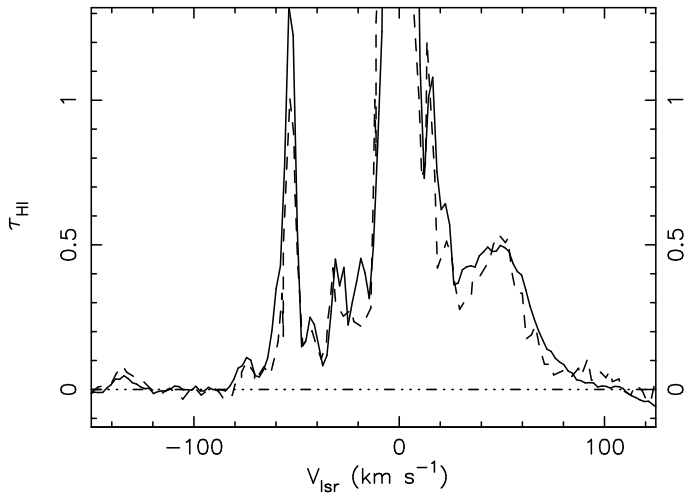

Fig. 4.4 The HI optical depth profi le towards the source SgrA from Radhakrishnan & Sarma (1980) (broken line) compared with our observation suitably convolved to match their bandwidth, velocity resolution and angular resolution (solid line).

		Parkes	ATCA
Baseline	:	120 m	1.5 km
Bandwidth	:	1.5 MHz	4.0 MHz
Velocity Resolution	:	2.1 km s^{-1}	0.8 km s^{-1}

To compare our conclusions with those obtained by Radhakrishnan and Sarma (1980), **we have smoothed our data to their velocity resolution and synthesized an image using the visibilities within a u-v range corresponding to 120 m from the ATCA observations. Only the data within the 1.5 MHz were used in imaging**. The comparison of the two is shown in Fig. 4.4. It may be seen that the two agree reasonably well. While Radhakrishnan and Sarma also found evidence for a shallow, wide absorption, the velocity width deduced by them, *viz.* 35 km s^{-1} is smaller than our estimate of $\sim$50 km s^{-1}. **We are of the opinion that the difference is attributable to the smaller bandwidth used by them**.

4.4.3 Comparison with the WSRT results

Schwarz, Ekers & Goss, 1982 used a 1.25 MHz bandwidth for their observations, with a velocity resolution of 4.1 km s^{-1} after Hanning smoothing and a synthesized beam of $23'' \times 143''$. They had a velocity coverage of –120 km $s^{-1} \lesssim V_{lsr} \lesssim$ +120 km s^{-1}. We have synthesized a spectral line cube to match these specifications. The comparison is shown in Figure 4.5. While there is an overall agreement, there are

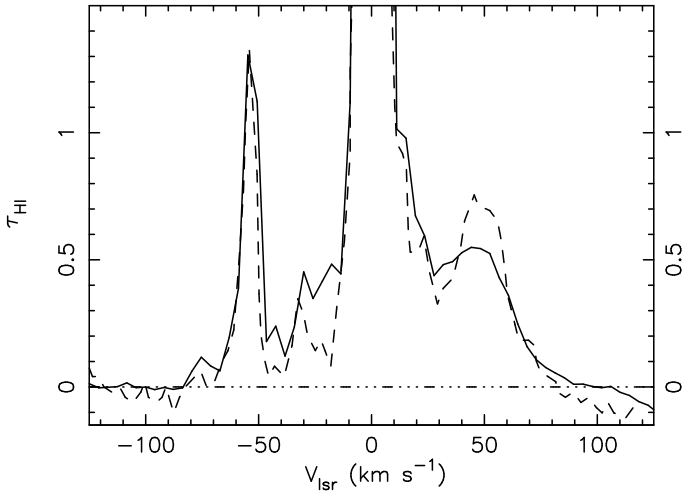

Fig. 4.5 The HI optical depth profi le towards the source SgrA from Schwarz, Ekers and Goss (1982) (broken line) compared with our observation suitably convolved to match their bandwidth, velocity resolution and angular resolution (solid line).

significant differences in the velocity ranges –10 to –50 km s^{-1} and +40 to +60 km s^{-1}.

As was noted earlier, the velocity spread in the HI absorption features towards SgrA is –180 km s^{-1} $\lesssim$ V$_{lsr}$ $\lesssim$ +125 km s^{-1} (Fig. 4.3a). We feel that the limited bandwidth used by Schwarz et al. has a serious implication for detecting any shallow, wide absorption feature. The narrower bandwidth used by them would have severely underestimated the absorption levels of *individual* features and hence resulted in the non-detection of the shallow wide component. Notice the shallow HI optical depth (Fig. 4.3a) with $\tau \sim 0.15$ at V$_{lsr}$ $\sim$ –100 km s^{-1} and at V$_{lsr}$ $\sim$ +100 km s^{-1}. These regions appear close to the edges of the band used by Schwarz et al and would have been considered as the spectral baseline. This is borne out by Fig. 4.5 in which our wide-band data convolved to the Schwarz et al. specification also does not reveal any significant absorption at $\pm$100 km s^{-1}. **In our opinion, the fact that the shallow wide absorption feature seen by us (centered at near zero velocity, with $\sigma_v \sim$ 50 km s^{-1}) was not clearly seen in the observations by Schwarz et al. due to the smaller bandwidth used by them.**

4.4.4 Results from the Galactic Anticenter observations

The only direction other than the Galactic Center where we can directly measure the peculiar motions of interstellar clouds is towards the Galactic Anticenter. This direction has relatively few HI absorption features as compared to the Galactic Center direction. Each of the observed fields showed two absorption features (Fig. 4.6 and

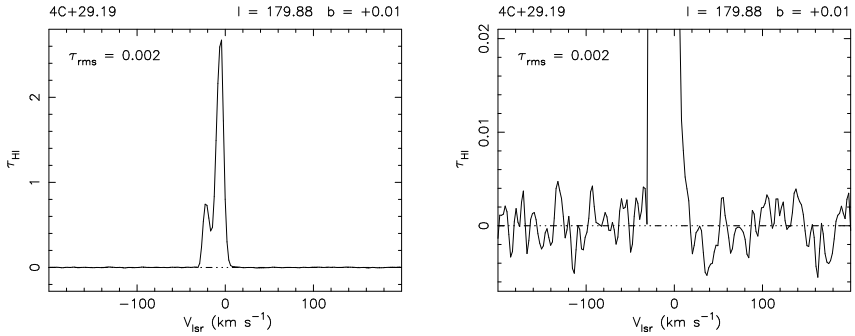

Fig. 4.6 HI optical depth profi le towards the source 4C +29.19 from the WSRT. First panel shows the full profi le and the second one shows an expanded y-scale.

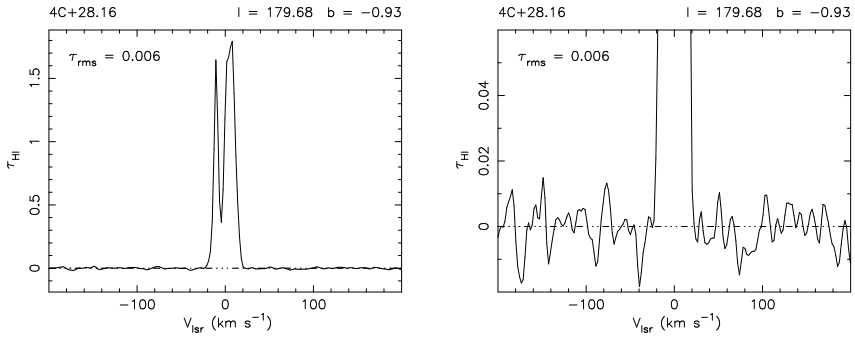

Fig. 4.7 HI optical depth profi le towards the source 4C +28.16 from the WSRT. First panel shows the full profi le and the second one shows an expanded y-scale.

Fig. 4.7). These two features are deep ($\tau_{HI} > 2$) and narrow ($\sigma_v \sim 3$ and 5 km s^{-1}). Gaussian fitting was carried out using the task XGAUPROF in GIPSY. Our efforts to identify the discrete HI absorption features in the profile using Gaussian fitting failed to perform a faithful fit. This can arise if there is severe blending. Such a situation can arise towards the Galactic anticenter, since this direction is free from any radial velocity component arising from the differential Galactic rotation. One can expect velocity crowding with all the narrow HI absorption features aligning one behind the other. In addition, as we mentioned earlier, HI self absorption is prominent in the Galactic plane, especially towards the directions like the Galactic center and Anticenter. Self absorption can result in non-gaussian features. However, from the figs 4.6 and 4.7, it is clear that no signature of a wide component is seen towards the Galactic Anticenter. Our observations set an upper limit to the HI optical depth of

any such feature, similar to the one identified towards the Galactic Center to be $<$ 0.006 (3σ), towards the source 4C +29.19.

4.5 DISCUSSION

The aim of the experiment described in this chapter was to resolve the controversy around the possible detection of a wide ($\sigma_v \sim$ 35 km s^{-1}) HI absorption feature detected towards the Galactic center in the Parkes Interferometer observations (Radhakrishnan and Sarma, 1980). This detection may be of prime importance in the study of the kinematics of HI clouds in the ISM if this feature is interpreted as arising from a global population of clouds, as was pointed out by Radhakrishnan and Srinivasan (1980). However, subsequent observations using the WSRT (Schwarz et al., 1982) failed to confirm this intriguing wide absorption feature. There were no further attempts to resolve this controversy. We have revisited this important but neglected problem by reobserving the Galactic center in the HI 21cm-line using the ATCA with a larger velocity coverage, and higher velocity resolution. We have also measured HI absorption towards two sources within a degree from the Galactic anticenter direction.

Our results are summarized below:

- **We have detected a wide ($\sigma_v \sim$ 50 km s^{-1}) HI absorption feature towards the Galactic center.**
- **This absorption feature is centered at V_{lsr} = 7 $\pm$ 2 km s^{-1} and has a peak HI optical depth $\sim$ 0.3**
- **The earlier WSRT Observations by Schwarz et al (1982) might have missed this feature due to the smaller bandwidth (1.25 MHz) used in their observations. The velocity spread in the HI absorption features towards the Galactic center is larger than the bandwidth used in their observations.**
- **The Parkes Interferometer observations (Radhakrishnan and Sarma, 1980) also had smaller bandwidth, but large enough to detect the shallow wide absorption. The smaller velocity width of $\sim$35 km s^{-1} derived by them might have been constrained by the smaller bandwidth.**
- **We have detected no wide absorption feature towards the Galactic anticenter, down to a 3σ limit of 0.006 in HI optical depth.**

Although the existence of the wide HI absorption line towards the Galactic center may have been resolved by the present observations, the non detection of such a feature towards the anticenter direction cast doubts regarding the interpretation of this as arising from a global population of anomalous velocity HI absorbing clouds, as suggested by Radhakrishnan and Srinivasan (1980). They had attributed the wide HI absorption feature to a population of weakly absorbing clouds, accelerated by

supernova remnants in their late phases of evolution.

The ATCA observations were carried out using 5 antennas, spread over a distance of $\sim$ 1.5 km. Though we find evidence for the wide line, it is impossible to study the spatial extent of the feature over the extended radio continuum emission in the Galactic center region. If this feature is arising due to a large number of clouds superposed along the line of sight towards the Galactic center, then one would expect the resulting HI absorption feature to be uniform over the radio continuum source SgrA. **The present ATCA observations do not have the required u-v coverage to undertake such a study**. At this juncture, we are unable to comment on how widespread the line is. To understand this more observations are required with better u-v coverage to image the Galactic center region in HI absorption.

The absence of such a feature towards the Galactic anticenter makes it more intriguing. One possibility is that the wide line is not related to a global population of large peculiar velocity clouds. The results from the HI absorption survey using the GMRT (chapter 3) did indicate the presence of two components in the velocity dispersion of radial velocities of HI absoption features. However, the number of higher velocity dispersion clouds were found to be only $\sim$ 20% of that of the low velocity clouds. Radhakrishnan & Srinivasan (1980) had estimated the number density (number per kiloparsec) of higher velocity clouds to be twice that of low velocity clouds.

Molecular clouds with similar large line widths ($\sigma_v \sim 50 - 80$ km s^{-1}) are indeed detected in the vicinity of the Galactic center. A large scale survey of OH absorption line by Boyce & Cohen (1994) in the Galactic center region has revealed several features with angular extent $\sim 0.5^o$ and large velocity dispersions (typically $\sim$ 60 km s^{-1}). Two of these features were imaged in HI 21cm-line emission by Riffert et al (1997). These clouds show unusually large velocity dispersion in the lines of ^{12}CO, ^{13}CO and CS molecules also. Kumar & Riffert (1997) tried to explain these velocity widths and after considering a number of possibilities concluded that cloud collisions are the most likely explanation. Therefore, the wide HI absorption line seen towards the Galactic center may be associated with one of these molecular clouds with large velocity dispersion (presumably the HI is associated with the outer regions of the clouds). Recently the Galactic center region was imaged in HI 21cm-line using the VLA. This observation detected such a wide line towards SgrA*, but may not be spatially extended (Dwarakanth, private communication). This is in favour of the conjecture that the wide line is presumably due to a single spatially confined feature.

4.6 CONCLUSIONS

To conclude, the present observation towards the Galactic Center provides evidence for a wide HI absorption feature with a $\sigma_v \sim 50$ km s^{-1} centered at V$_{lsr}$ = $+7 \pm 2$ km s^{-1}. Our results are consistent with the conclusions arrived at from an analysis of

the Parkes Interferometer observations (Radhakrishnan and Sarma, 1980). However, they underestimated the width of this line ($\sigma_v \sim 35$ km s^{-1}) due to their limited (316 km s^{-1}) bandwidth. The bandwidth (264 km s^{-1}) used in the observations of Schwarz et al (1982) was inadequate to detect this wide feature. Given the large velocity spread (–180 km s^{-1} $\lesssim$ V$_{lsr}$ $\lesssim$ +125 km s^{-1}) of the HI absorption features towards the source SgrA, the wide bandwidth (845 km s^{-1}) and the high velocity resolution (0.8 km s^{-1}) used in the current observations are critical in disentangling the plethora of narrow HI absorption lines to reveal the underlying wide HI absorption line. However, the absence of a similar wide line towards the Galactic anticenter warrants more attention. A global population of large velocity clouds would have resulted in the detection of wide line towards both the Galactic center as well as the anticenter. An alternative scenario is more likely. There exists a number of cases of individual molecular clouds in the vicinity of the Galactic center with unusually large HI/OH/CO line widths. It is possible that the wide HI line seen towards the Galactic center is arising in one of these clouds. However, the present study is unable to resolve this.

REFERENCES

1. Adams, W.S., 1949, Astrophys. J. 109 354.
2. Anantharamaiah, K.R., Radhakrishnan, V., Shaver, P.A., 1984, Astron. Astrophys. 138 131.
3. Balick, B., Brown, R.L., 1974, Astrophys. J. 194 265.
4. Blaauw, A., 1952, Bull. Astr. Inst. Netherlands. 11 459.
5. Bower, G.C., Backer, D.C., 1998, Astrophys. J. Lett. 496 L97.
6. Boyce, P.J., Cohen, R.J., 1994 Astron. Astrophys. Suppl. 107 563.
7. Coil, A.L., Ho, Paul T.P., 1999, Astrophys. J. 513 752.
8. Crovisier, J., 1978, Astron. Astrophys. 70 43.
9. Hartmann, D., Burton, W.B., 1995, An Atlas of Galactic Neutral Hydrogen Cambridge Univ. Press, Cambridge.
10. Genzel, R., Thatte, N., Krabbe, A., Kroker, H., Tacconi-Garman, L. E., 1996, Astrophys. J. 472 153.
11. Kulkarni, S.R., Fich, M. 1985, Astrophys. J. 289 792.
12. Kumar, P., Riffert, H., 1997, MNRAS 292 871.

13. Liszt, H.S., Van der Hulst, J.M., Burton, W.B., Ondrechen, M.P., 1983, Astron. Astrophys. 126 341.

14. Pedlar, A., Anantharamaiah, K.R., Ekers, R.D., Goss, W.M., van Gorkom, J.H., Schwarz, U.J., Zhao, Jun-Hui, 1989, Astrophys. J. 342 769.

15. Press, W.H., Teukolsky, S.A., Vetterling, W.T., Flannery, B.P., 192, Numerical Recipes, The Art of Scientific Computing Cambridge Univ. Press, Cambridge.

16. Radhakrishnan, V., Goss, W.M., Murray, J.D., Brooks, J.W., 1972, Astrophys. J. Suppl. 24 49.

17. Radhakrishnan, V., Sarma, N.V.G., 1980, Astron. Astrophys. 85 249.

18. Radhakrishnan, V., Srinivasan, G., 1980, J. Astrophys. Astroon. 1 47.

19. Rajagopal, J., Srinivasan, G., Dwarakanath, K.S. 1998, J. Astrophys. Astron. 19 97.

20. Riffert, H., Kumar, P., Huchtmeier, W.K., 1997, MNRAS 284 749.

21. Roberts, D.A., Yusef-Zadeh, F., Goss, W.M., 1996, Astrophys. J. 459 627.

22. Routly, P.M., Spitzer, L. Jr. 1952, Astrophys. J. 115 227.

23. Schwarz, U.J., Ekers, R.D., Goss, W.M., 1982, Astron. Astrophys. 110 100.

24. Serabyn, E., Lacy, J.H., Achtermann, J.M., 1992, Astrophys. J. 395 166.

25. Siluk, R.S., Silk, J., 1974, Astrophys. J. 192 51.

26. Yusef-Zadeh, F., Morris, M., 1987, Astrophys. J. 320 545.

27. Yusef-Zadeh, F., Morris, M., van Gorkom, J. H., 1989, in The Center of the Galaxy, Proc. IAU Symp. 136 eds. Mark Morris, Dordrecht: Kluwer Acad. Publ., pp 275.